A&A 534, A65 (2011)
DOI: 10.1051/0004-6361/201117356

Astronomy & Astrophysics

MHD wave transmission in the Sun's atmosphere

M. Stangalini[1], D. Del Moro[1], F. Berrilli[1], and S. M. Jefferies[2]

[1] Dipartimento di Fisica, Università di Roma "Tor Vergata", via della Ricerca Scientifica 1, 00133 Rome, Italy
e-mail: marco.stangalini@roma2.infn.it
[2] University of Hawai'i, Institute for Astronomy, 34 "Ohi"a Ku St. Pukalani, Hawaii 96768-8288, USA

Received 27 May 2011 / Accepted 20 August 2011

ABSTRACT

Magnetohydrodynamics (MHD) wave propagation inside the Sun's atmosphere is closely related to the magnetic field topology. For example, magnetic fields are able to lower the cutoff frequency for acoustic waves, thus allowing the propagation of waves that would otherwise be trapped below the photosphere into the upper atmosphere. In addition, MHD waves can be either transmitted or converted into other forms of waves at altitudes where the sound speed equals the Alfvén speed. We take advantage of the large field-of-view provided by the IBIS experiment to study the wave propagation at two heights in the solar atmosphere, which is probed using the photospheric Fe 617.3 nm spectral line and the chromospheric Ca 854.2 nm spectral line, and its relationship to the local magnetic field. Among other things, we find substantial leakage of waves with five-minute periods in the chromosphere at the edges of a pore and in the diffuse magnetic field surrounding it. By using spectropolarimetric inversions of Hinode SOT/SP data, we also find a relationship between the photospheric power spectrum and the magnetic field inclination angle. In particular, we identify well-defined transmission peaks around 25° for five-minute waves and around 15° for three-minute waves. We propose a very simple model based on wave transmission theory to explain this behavior. Finally, our analysis of both the power spectra and chromospheric amplification spectra suggests the presence of longitudinal acoustic waves along the magnetic field lines.

Key words. Sun: oscillations – magnetohydrodynamics (MHD) – Sun: surface magnetism – Sun: helioseismology

1. Introduction

The source of the energy needed to heat the Sun's corona is a long-standing enigma. The two main competing theories proposed to explain the energy excess in the outer atmosphere of the Sun are Joule heating through resistive dissipation by magnetic field reconnection and mechanical heating by waves (see Aschwanden 2001, for a review of the mechanisms proposed). However, both Joule heating and mechanical heating by high-frequency acoustic waves ($\nu_c > 5.2$ mHz) have been ruled out as major contributors to the energy budget of the corona (Fossum & Carlsson 2006; Spangler 2009). Low-frequency MHD waves ($\nu < 5$ mHz), on the other hand, may represent a significant source of energy (Jefferies et al. 2006). Although these waves are generally not allowed to propagate into the atmosphere, because their frequency does not exceed the expected photospheric cutoff frequency ($\nu_c = 5.2$ mHz), in regions where the magnetic field is largely inclined with respect to the gravity vector the cutoff frequency can be lowered by means of the ramp effect

$$\omega_{\rm eff} = \omega_c \cos\theta, \tag{1}$$

where $\omega_{\rm eff}$ is the effective cutoff frequency and θ is the angle of the magnetic field to the local gravity vector. This effect is behind the so-called magneto-acoustic portals (Jefferies et al. 2006) that allow waves with frequencies far below 5.2 mHz to be channeled into the strongly inclined magnetic field.

It has been demonstrated both theoretically (Schunker & Cally 2006; Cally & Goossens 2008) and through numerical simulations (Khomenko & Collados 2006; Felipe et al. 2010), that at locations where the sound speed c_s and Alfvén speed a nearly coincide, part of the energy contained in the acoustic-like component (fast MHD mode in the $\beta > 1$ regime) can be converted into two types of waves: field-aligned acoustic waves (slow MHD mode in $\beta < 1$ plasma), or magnetic-like waves (fast mode in $\beta < 1$ regions). These two processes are commonly referred to as "fast-to-slow" and "fast-to-fast" conversions. In the first case, the acoustic nature of the wave is preserved, while in the fast-to-fast conversion, the wave changes from acoustic-like to magnetic-like. We note that since $c_s^2/a^2 = (\gamma/2)\beta$, the layer where the gas pressure is equal to the magnetic pressure (the $\beta = 1$ or equipartition layer) is in practice very close to the layer where the phase speed of the fast and slow modes coincide, even if they are conceptually different. The amount of energy transferred to the acoustic-like mode or converted into the magnetic-like mode, as the wave crosses the equipartition layer, depends on the angle between the wavevector and the magnetic field (the attack angle α)

$$T = \exp[-\pi k h_s \sin^2\alpha], \tag{2}$$

where h_s is the thickness of the equipartition layer as measured along the direction of propagation, in which the process of mode conversion is taking place, k is the wavenumber, and T is the "fast-to-slow" transmission coefficient. We note that this relation is strictly valid only for small attack angles, and that a comparison with the exact solution can be found in Hansen & Cally (2009). The "fast-to-fast" transmission coefficient C is obtained by invoking conservation of energy, i.e.

$$T + |C| = 1 \tag{3}$$

and C is complex (as we need to take into account possible phase changes during conversion). Schunker & Cally (2006) demonstrated that the ramp and mode conversion effects together result in a strong dependence of the acoustic energy flux on both the magnetic field inclination and the attack angle. In particular, the acoustic flux should have a maximum for magnetic field inclination angles between 20 and 30 degrees. This is a result of the

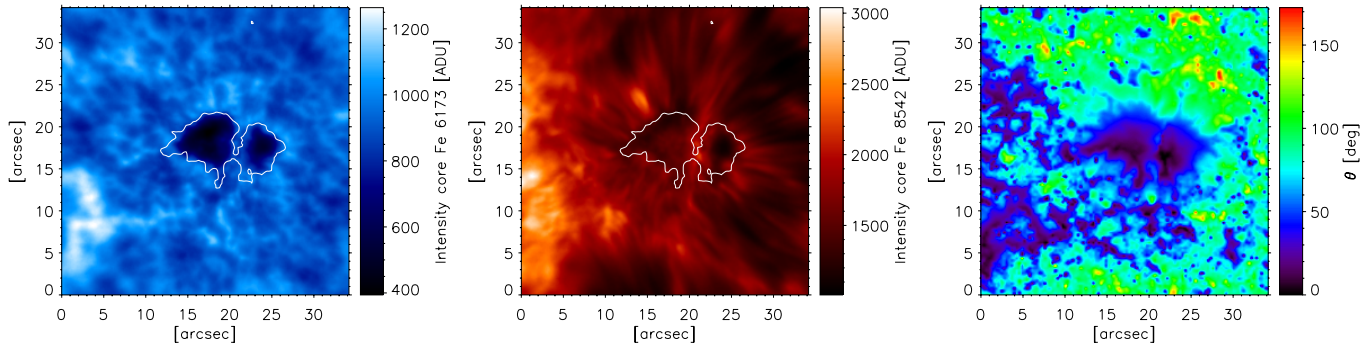

(a) Core Fe 617.3 nm (b) Core Ca 854.2 nm (c) θ @ 300 km

Fig. 1. a) IBIS intensity image in the core of the Fe 617.3 nm photospheric line. **b)** IBIS intensity image in the core of the Ca 854.2 nm chromospheric line. **c)** Magnetic field inclination in the photosphere as inferred from MERLIN inversions on Hinode data.

transmission coefficient being large at smaller attack angles and the ramp effect allowing the propagation of low frequency waves once $\cos\theta < \omega_{\rm eff}/\omega_{\rm c}$, that is at large inclination angles. Here we investigate this claim and show how the velocity field fluctuations of a solar active region observed by the Interferometric BIdimensional Spectrometer (IBIS) based on a dual Fabry-Perot system, depend on the inclination angle of the magnetic field, as inferred from the spectropolarimetric inversions of the same region observed by Hinode SOT/SP (Tsuneta et al. 2008).

Among other things, we find that the power of the velocity oscillations depends on both the frequency and the magnetic field inclination: this is in accord with the above theoretical picture. This scenario is also supported by the analysis of the spatial distribution of the power in the chromosphere, which shows that there is a substantial lack of power at the locations where the magnetic field is bent horizontally. This is consistent with longitudinal waves moving along the field lines, these waves being undetectable when they propagate parallel to the line-of-sight.

2. Observations

The data used in the work were acquired on 2008 October 15 at 16:30 UT in full Stokes mode with IBIS at the Dunn Solar Telescope. The experiment combined high-spectral resolution with short exposure times and a large field of view, as well as the ability to measure polarization (Cavallini 2006).

The region observed was AR11005. This region, as seen by both SOHO and Hinode images, appears as a small pore with a light bridge in the northern hemisphere at high latitude [25.2° N, 10.0° W], hence is very likely to belong to solar cycle 24.

The dataset consists of 80 sequences of measurements, each containing a 21 point scan of the full Stokes vector for both the Fe 617.3 nm and Ca 854.2 nm lines. The difference in wavelength between the spectral points for the Fe line was 2 pm. The exposure time for each image was set to 80 ms and each spectral scan took 52 s to complete. The pixel scale of these 512×512 images was set at 0.167 arcsec. For each spectral image, we also acquired a broad-band (WL) and a G-band counterpart, both imaging approximately the same FoV. The pixel scale of the 1024×1024 WL image (621.3 ± 5 nm) was set at 0.083 arcsec and the exposure time was 80 ms (shared shutter with IBIS spectral images). The pixel scale of the 1024×1024 G-band image (430.5 ± 0.5 nm) was set at 0.051 arcsec and the integration time was 10 ms.

The ancillary images were restored with multi-frame blind deconvolution (MFBD) (van Noort et al. 2005), resulting in a single frame for each scan for both the G-band and the broad-band images. Using these restored images, the spectropolarimetric images were registered and destretched to minimize the seeing effects uncorrected by the AO and to achieve the highest spatial resolution.

The pipeline for IBIS data reduction takes care of normal calibration processes (dark frame, flat field, etc.) and also corrects for blue-shift effects (Reardon & Cavallini 2008) and instrumental polarization: the latter is important for minimizing residual cross-talk between the Stokes profiles. For further details of the calibration pipeline, we refer to Viticchié et al. (2009).

The estimated mean spatial resolution of the line-of-sight (LoS) velocity fields computed from the spectropolarimetric scans used in this work is 0.36 arcsec.

In addition to IBIS data, we also used Hinode SOT/SP observations of the same active regions taken three and half hours before the IBIS data set.

2.1. Ca 854.2 nm and Fe 617.3 nm formation heights

When dealing with waves, it is essential to know the formation heights of the spectral lines and their position with respect to the equipartition layer (namely the layer in which the MHD mode conversion takes place). As mentioned earlier, IBIS observations were obtained using two spectral lines: the chromospheric Ca 854.2 nm and the photospheric Fe 617.3 nm.

As for the Ca 854.2 nm line, Cauzzi et al. (2008) and Vecchio et al. (2009) pointed out that this spectral line spans a wide range of atmospheric heights starting from the mid-high photosphere to the low chromosphere (line core).

Norton et al. (2006) estimated the quiet Sun height of formation of the Fe 617.3 nm core to be around 300 km above the photosphere. This has to be compared with the altitude of the equipartition layer in our region of interest in order to estimate the plasma β regime sampled by our observations. To achieve this aim, we estimated the equipartition layer position using spectropolarimetric inversions obtained using the SIR code (Ruiz Cobo & del Toro Iniesta 1992) performed on SOT/SP data. Our estimate reveals that the equipartition layer is slightly below the height of formation of the Fe 617.3 nm spectral line throughout the FoV, implying that we observe the onset of the low-β regime in the solar atmosphere, very close to the conversion altitude.

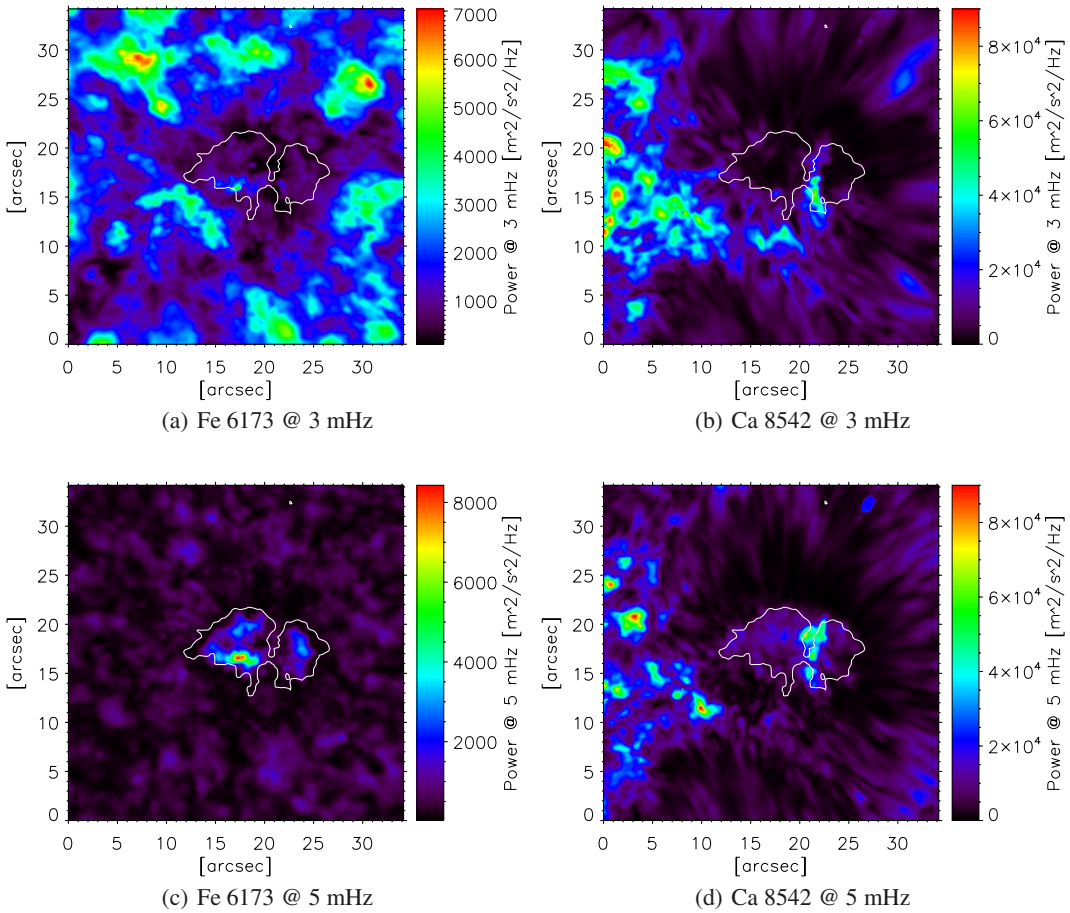

(a) Fe 6173 @ 3 mHz (b) Ca 8542 @ 3 mHz

(c) Fe 6173 @ 5 mHz (d) Ca 8542 @ 5 mHz

Fig. 2. a) IBIS Fe 617.3 nm power map at 3 mHz. **b)** IBIS *Ca* 854.2 nm power map at 3 mHz. **c)** IBIS Fe 617.3 nm power map at 5 mHz. **d)** IBIS Ca 854.2 nm power map at 5 mHz. Continuous contours indicate approximatively the position of the umbra.

2.2. Inclination angle at photospheric and chromospheric heights

As previously mentioned, we explore here the characteristics of the power spectral density at different magnetic field inclinations with respect to the local gravity vector. This is done by comparing the information encoded in the temporal sampling to the spectropolarimetric data provided by the Hinode SOT spectropolarimeter.

Using MERLIN inversions, we studied maps of inclination of the same region observed with IBIS a few hours later. Hinode SOT/SP Inversions were conducted at NCAR under the framework of the Community Spectropolarimtetric Analysis Center (CSAC). The result is shown in Fig. 1. In Fig. 3 (panel d), we show the chromospheric magnetic field inclination obtained from non-linear force-free extrapolations performed using the NLFF code (De Rosa et al. 2009), after resolving the azimuth ambiguity by means of the code presented in Leka et al. (2009)[1]. Even though the low chromosphere is not a place where the force-free approximation holds, the observational results obtained in this work can easily be explained by our extrapolated model, suggesting the validity of such a scheme even in this context.

[1] Further details about the code can be found at http://www.cora.nwra.com/AMBIG/.

3. Results

We now focus on the analysis of the velocity field perturbations in two power spectral bands namely 2.8−3.8 mHz and 4.8−5.8 mHz, hereafter the five-minute and three-minute bands respectively.

Due to the limited extent of the time series data, the use of the FFT to estimate the power spectral density may result in a distorted estimation (Edge & Liu 1970). For this reason, we estimate the power spectral density using the Blackman-Tukey method and use a Barlett windowing function (Blackman & Tukey 1958).

3.1. Photospheric power spectral density

Figure 2 shows the power maps for the three and five-minute bands sampled by the Fe 617.3 nm line (panels a and c, respectively).

The power distribution in the two spectral bands look quite different. The five-minute oscillations tend to be spread throughout the FoV, while they are absent (absorbed) in the magnetic region. This is unsurprising and a long series of similar results can be found in the literature (see Chou et al. 2009, and references therein). The magnetic field is, in fact, able to scatter and absorb the acoustic field thus producing such an effect. On the other hand, three-minute oscillations are only found in the umbra of the pore.

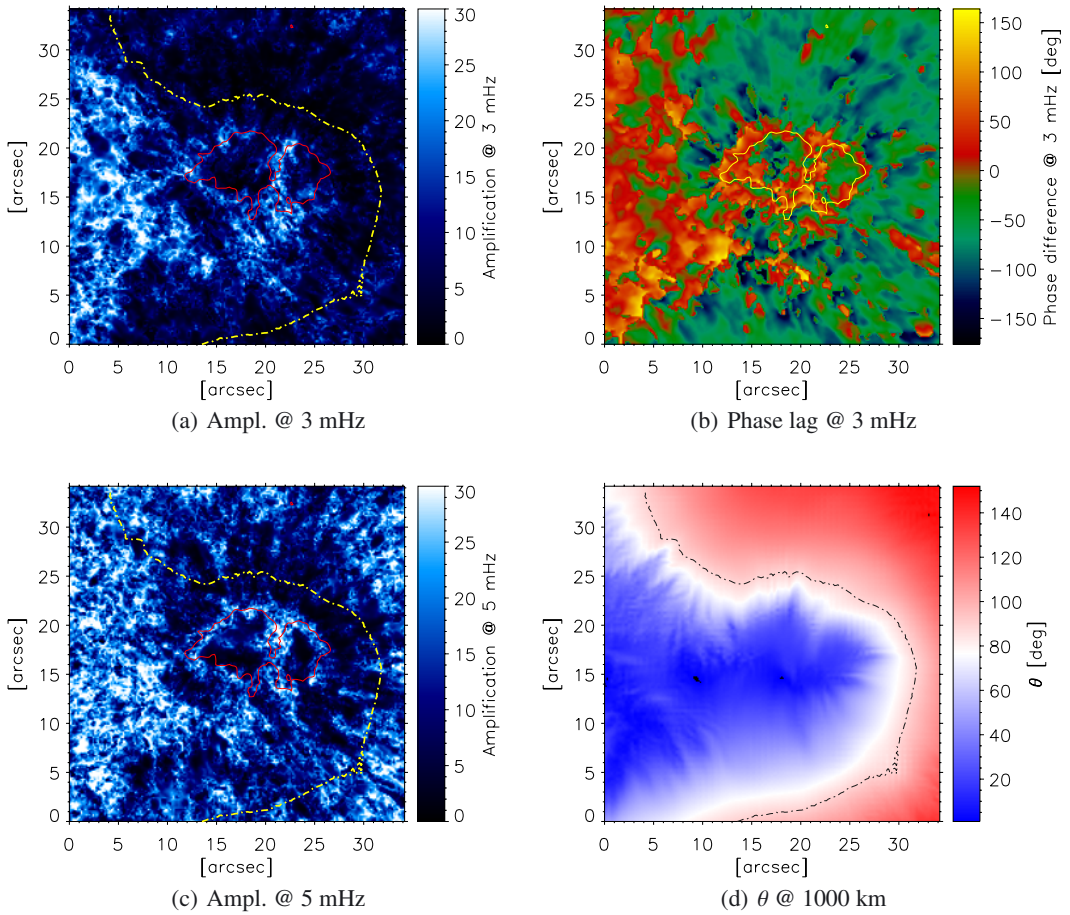

(a) Ampl. @ 3 mHz (b) Phase lag @ 3 mHz

(c) Ampl. @ 5 mHz (d) θ @ 1000 km

Fig. 3. a) Amplification map at 3 mHz from IBIS data. **b)** Phase lag between photosphere and chromosphere at 3 mHz (positive values mean upward propagation) from IBIS data. **c)** Amplification map at 5 mHz from IBIS data. **d)** Chromospheric magnetic field inclination as inferred from extrapolations of the Merlin magnetic vector map of Hinode data. Continuous contours approximatively indicate the position of the umbra, and dashed contours in the amplification maps indicate the position where the chromospheric magnetic field is 90 degrees inclined with respect to the LoS.

3.2. Chromospheric power spectral density

The chromospheric power maps in the five-minute and three-minute bands (panels b and d of Fig. 2) are even more noticeable and interesting than their photospheric counterparts. What is clear in these maps is the strong presence of five-minute oscillations in both the diffuse magnetic field and the light bridge.

What is even more interesting is the absence of power in an annulus surrounding the spot. Our interpretation of this mechanism is that the slanted nature of the longitudinal waves running along the field lines makes them invisible to a line-of-sight observation. This agrees, of course, with the general view that describes the magnetic field as acting as a filter on the transmitted waves, permitting in particular the passage of waves more aligned with the field lines themselves (Cally 2006).

3.3. Chromospheric amplification

In accord with the conservation of energy, the amplitude of acoustic waves increases with height in the atmosphere because of the rapid decrease in density with increasing height. Moreover, these waves are subject to non-linear steepening leading to the formation of shocks (Vecchio et al. 2009). It is therefore interesting to study the nature of this growth in amplitude as it may reveal important details about the density stratification of the atmosphere overlying the photospheric magnetic structure. It may also provide valuable information about the energy deposition brought by waves in the low/mid chromosphere.

We analyzed the structure under investigation by taking the ratio of the chromospheric to photospheric power spectral density in both frequency bins. In the case of waves above the cut-off frequency, we generally expect to see an upward propagation toward the chromosphere, hence it is unsurprising to find a power amplification everywhere in the FoV as shown by Fig. 3 for the three-minute waves (panel c). What is equally interesting in the map is the clear evidence of a lack of amplification in the region surrounding the umbra in both spectral bands. We interpret this as evidence of slow longitudinal magneto-acoustic modes running preferentially along slanted magnetic field lines. This behavior is still present in the five-minute band, even though it is less evident. The dashed lines in panels *a* and *c* of Fig. 3 indicate the 90° isocontour of the LoS chromospheric magnetic field inclination estimated using the field extrapolations discussed above, and corrected for the position of the region on the solar disk. As the magnetic field lines become highly inclined with respect to the LoS, the velocity field fluctuations disappear as they are longitudinal, producing an "absorption" halo in our chromospheric power and consequently in the amplification maps. We note that the absorption halo surrounding the spot and the

90° chromospheric inclination isocontours match perfectly, especially for three-minute waves, although they came from independent estimates, namely power spectra analyses and magnetic field extrapolations.

Moreover, the amplification of the five-minute waves is not present throughout the FoV but is concentrated in the small magnetic elements and on the edge of the umbra. As for the small magnetic elements, this effect appears to be evidence of a decrease in the cut-off frequency caused by radiative losses (Khomenko et al. 2008), which allows the channeling of five-minute power in the low chromosphere even in vertical magnetic fields. This agrees with previous analyses of the chromospheric power spectra in small magnetic flux tubes (Centeno et al. 2009). On the other hand, the chromospheric amplification at the edge of the umbra can be interpreted as a lowering of the cut-off frequency caused by magnetic field inclination (Jefferies et al. 2006).

3.4. Propagation of five-minute waves toward the chromosphere: phase spectra

One of the main advantages of dual-line investigations of the solar atmosphere, is the possibility to study the vertical behavior of waves and search for upwardly propagating components. For this purpose, we used a phase difference analysis.

Fe 617.3 nm and Ca 854.2 nm lines are scanned sequentially in about 52s, hence when estimating the phase lag, using the FFT cross-correlation, we took into account the time lag between the two scans of the lines, and corrected the phase lag maps accordingly. The results of this analysis for the 5-min band is shown in panel *b* of Fig. 3. In our sign convention, positive values of the phase lag mean that the chromospheric signal lags behind the photospheric one, thus representing an upward propagation.

Similar to the amplification maps, the phase maps indicate that a lot of five-minute waves reach the formation height of the Ca 854.2 nm.

3.5. Power as a function of magnetic field inclination

To investigate the properties of the magnetic field inclination in terms of wave transmission/conversion, we compared the periodogram of the observed perturbations with the photospheric inclination of the magnetic field estimated by the inversions performed on the same active region observed by Hinode/SOT.

In particular, we chose different regions over the FoV, pertaining to different magnetic field angles to the vertical. For each of these regions, we estimated the maximum of the power averaged over a six-degree interval, using the Welsch method, for different magnetic field inclinations. Before performing the analysis, the Hinode and IBIS data sets were co-registered to sub-pixel accuracy using a technique based upon FFT cross-correlation.

A visual inspection of the resulting co-registration shows that there is a very close match between the two data-sets despite being acquired three-and-a-half hours apart. This suggests that at least the strong magnetic field structures are quite stable over time, and that the evolutionary time scales are much longer than the time interval between the acquisition of each data set. This further proves the feasibility of our investigation when comparing Hinode inversions with the dynamics sampled by IBIS. We assume that the inclination angle is equal to the attack angle between the incoming acoustic waves wave-vector and the magnetic field lines themselves. Once again we selected

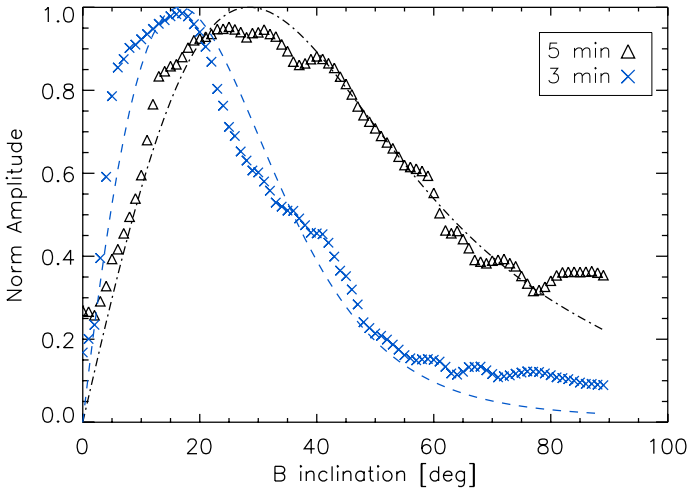

Fig. 4. Transmission in the three and five minute bands as a function of magnetic field inclination from IBIS data. Dashed and dot-dashed curves represent the result of the fit of our model, for three and five minute bands respectively.

two representative spectral bands around three and five minutes. Figure 4 shows the integrated power in the two selected spectral bands as a function of magnetic field inclination. The most striking result of this analysis is the dependence of the power upon the magnetic field geometry. This result supports the predictions of the model proposed by Schunker & Cally (2006).

3.6. A simple model

The transmission of the five- and three-minute acoustic waves depends strongly on the attack angle, which acts as a filter.

To help us understand this behavior, we propose a simple model consisting of three components related to the transmission coefficient, the ramp effect, and the geometrical projection effects. Before going into any detail about these terms and their contribution to our model, we introduce a modified transmission relation

$$T = \exp\left[-\pi k h_s \sin^2\theta\right]\left[1-\exp\left(-\frac{\theta}{\theta_c}\right)\right]\cos\,(\theta-\theta_{pos}), \qquad (4)$$

where θ_{pos} is the heliocentric angle taking into account projection effects. As discussed above, the first exponential term represents the transmission coefficient from fast (acoustic) to slow (acoustic) waves. These waves are generally longitudinal waves showing a slanted propagation along the field lines. For this reason, as the magnetic field bends toward the horizontal we do not expect these waves to be readily detectable, hence we add a $\cos(\theta-\theta_{pos})$ term to take into account the power suppression due to the projection effects. In doing this, we assume that the most important contribution is given by longitudinal acoustic waves. The middle term models the ramp effect, that is, the lowering of the cut-off frequency due to the magnetic field inclination. For inclination angles larger than a critical value θ_c, we begin to see transmission. We then estimate the critical angle using

$$\theta_c = \cos\,(\nu/\nu_c)^{-1}, \qquad (5)$$

where ν_c is the quiet Sun acoustic cutoff frequency set to 5.2 mHz.

Figure 4 shows the normalized transmission amplitude as a function of inclination angle superimposed on the trend expected

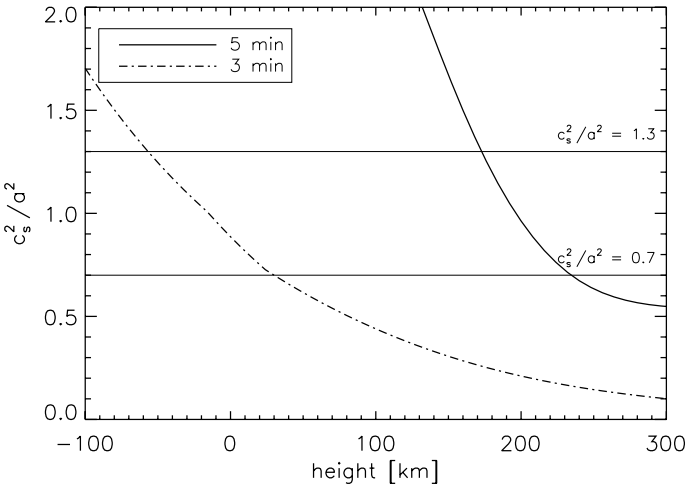

Fig. 5. Estimates of the ratio c_s^2/a^2 in the same regions selected for the analysis of the transmission obtained by means of SIR spectropolarimetric inversions of Hinode data. The region emitting five-minute waves show a steeper c_s^2/a^2 ratio, suggesting a smaller conversion layer thickness.

from the model (dashed lines). Interestingly, using the model itself, we can estimate the width of the layer in which the conversion is taking place (the h_s parameter). It appears that this parameter is different for the five-minute and three-minute waves.

From a least squares fit to our data, we found that h_s = 242 km for the three-minute waves and 203 km for the 5-min waves, with a reduced χ^2 = 0.0068 and χ^2 = 0.0052, respectively.

The reason for this difference is found in the different spatial location of the two kinds of waves. As shown in Fig. 3 and commented above, three-minute waves and five-minute waves are not co-spatial, the former are mainly located inside the umbra of the pore, while the latter are located in both the surrounding region and the diffuse magnetic field. The conversion layer thickness depends on the slope of the c_s^2/a^2 ratio, hence on the local atmospheric conditions. Our estimates of the h_s parameter suggest that in the umbral region, where the power of the three-minute waves can be clearly seen, the slope of c_s^2/a^2 is smaller than that associated with the five-minute waves, thus the conversion layer for the three-minute waves is thicker.

To independently confirm that, we estimated the shape of the c_s^2/a^2 function in the same regions selected for the analysis of the transmission, by using SIR spectropolarimetric inversion code (Ruiz Cobo & del Toro Iniesta 1992) to produce an atmospheric model starting from the Hinode data set. The results of this analysis is reported in Fig. 5, and clearly illustrate that the the above mechanism is valid.

The regions emitting five-minute waves have a steeper c_s^2/a^2, thus suggesting a smaller conversion layer thickness with respect to the regions emitting three-minute waves (the umbral region), where the thickness is larger.

4. Discussion

The results presented so far point to a fairly self-consistent picture in which the amount of energy provided by waves in the upper Sun's atmosphere depends strongly on the magnetic field topology. Our results also suggest that most of the waves transmitted in the chromosphere are longitudinal waves, that is slow (acoustic-like) MHD waves in a low-β atmosphere whose signatures disappear from our LoS as the magnetic field lines become highly inclined. We believe that this interpretation is supported by the maps of the chromospheric power and the amplification showing a clear absorption in those regions where the magnetic field is inclined by 90° with respect to the LoS.

With this in mind, we have been able to modify the transmission coefficient for acoustic waves crossing the equipartition layer in the solar atmosphere to provide a simple model for our results.

Our model is able to reproduce fairly well the observed dependence of the power on the magnetic field photospheric inclination angle for both five-minute and three-minute waves once the local modification of the cut-off frequency is taken into account. This provides us with an estimate of the thickness of the equipartition layer in which the mode conversion takes place (h_s = 200−240 km).

As highlighted by Schunker & Cally (2006), the magnetic field causes the helioseismic waves to split into fast and slow magnetoacoustic branches and it causes the waves to be progressively more field-aligned. Our results suggest that in the chromosphere, most of the energy contribution made by the waves is in the slow acoustic mode, that is longitudinal and field-aligned waves.

Moreover, we find a small discrepancy in the estimate of the equipartition layer thickness that can be explained by the different slopes of the c_s^2/a^2 as a function of height corresponding to the selected regions, as inferred from spectropolarimetric inversions. We conclude that this provides a further test of the validity of our model. Since the five-minute waves and the three-minute waves are not co-spatial, they reflect the changes in the atmosphere in which they propagate.

5. Conclusions

We have addressed the problem of wave transmission in different magnetic field inclination regimes in the solar atmosphere. This problem has been investigated by means of IBIS multi-height observations and by modeling them with a general theoretical picture based upon fast-to-slow transmission theory.

Our results clearly underline the presence of a strong connection between wave transmission and magnetic field geometry. Using spectropolarimetric IBIS data, we have studied the behavior of the photospheric power in two spectral bands, namely five and three minutes, with the inclination angle of the observed magnetic field, as inferred from Merlin inversions of Hinode data. We found that the power is not equally distributed but peaks at certain angles of inclination: around 25° for five minute and 15° for three minute waves.

Using a basic model that includes a fast to slow transmission term, projection effects expected in the presence of longitudinal waves, and the so-called ramp effect, we have been able to reproduce the observational signature of the power as a function of the inclination angle. This has revealed that most of the waves observed in the photosphere are longitudinal acoustic waves characterized by a slanted propagation along the field lines.

This scenario is also supported by the power spectrum analysis at both photospheric and chromospheric layers, which reveals an evident lack of both power and amplitude amplification in regions where the field lines are expected to be inclined at 90° to the LoS. This emphasizes that the lack of any wave signature is due to the presence of longitudinal waves (slow MHD mode in low-β chromospheric plasma).

We have found upwardly propagating waves in both five and three minute bands able to reach to chromosphere. This happens

predominantly at the edges of the magnetic umbra and in the diffuse surrounding magnetic field.

Acknowledgements. We acknowledge the support of Fabio Giannattasio in performing the SIR inversions of Hinode data. We also kindly thank the HAO-CSAC team for mantaining access to the Merlin inversion client. IBIS was built by INAF-Osservatorio Astrofisico di Arcetri with contributions from the Università di Firenze and the Università di Roma "Tor Vergata". Hinode is a Japanese mission developed and launched by ISAS/JAXA, collaborating with NAOJ as a domestic partner, NASA and STFC (UK) as international partners. Scientific operation of the Hinode mission is conducted by the Hinode science team organized at ISAS/JAXA. This team mainly consists of scientists from institutes in the partner countries. Support for the post-launch operation is provided by JAXA and NAOJ (Japan), STFC (UK), NASA, ESA, and NSC (Norway).

References

Aschwanden, M. J. 2001, ApJ, 560, 1035
Blackman, R., & Tukey, J. 1958, The measurement of power spectra from the point of view of communications (Dover Publications)
Cally, P. 2006, Phil. Trans. Roy. Soc. A: Math. Phys. Eng. Sci., 364, 333
Cally, P. S., & Goossens, M. 2008, Sol. Phys., 251, 251
Cauzzi, G., Reardon, K. P., Uitenbroek, H., et al. 2008, A&A, 480, 515
Cavallini, F. 2006, Sol. Phys., 236, 415
Centeno, R., Collados, M., & Trujillo Bueno, J. 2009, ApJ, 692, 1211
Chou, D., Yang, M., Zhao, H., Liang, Z., & Sun, M. 2009, ApJ, 706, 909
De Rosa, M. L., Schrijver, C. J., Barnes, G., et al. 2009, ApJ, 696, 1780
Edge, B. L., & Liu, P. C. 1970, Water Resour. Res., 6, 1601
Felipe, T., Khomenko, E., & Collados, M. 2010, ApJ, 719, 357
Fossum, A., & Carlsson, M. 2006, ApJ, 646, 579
Hansen, S. C., & Cally, P. S. 2009, Sol. Phys., 255, 193
Jefferies, S. M., McIntosh, S. W., Armstrong, J. D., et al. 2006, ApJ, 648, L151
Khomenko, E., & Collados, M. 2006, ApJ, 653, 739
Khomenko, E., Centeno, R., Collados, M., & Trujillo Bueno, J. 2008, ApJ, 676, L85
Leka, K. D., Barnes, G., & Crouch, A. 2009, in The Second Hinode Science Meeting: Beyond Discovery-Toward Understanding, ed. B. Lites, M. Cheung, T. Magara, J. Mariska, & K. Reeves, ASP Conf. Ser., 415, 365
Norton, A. A., Pietarila Graham, J. D., Ulrich, R. K., et al. 2006, in ASP Conf. Ser. 358, ed. R. Casini, & B. W. Lites, 193
Reardon, K. P., & Cavallini, F. 2008, A&A, 481, 897
Ruiz Cobo, B., & del Toro Iniesta, J. C. 1992, ApJ, 398, 375
Schunker, H., & Cally, P. S. 2006, MNRAS, 372, 551
Spangler, S. R. 2009, Nonlin. Process. Geophys., 16, 443
Tsuneta, S., Ichimoto, K., Katsukawa, Y., et al. 2008, Sol. Phys., 249, 167
van Noort, M., Rouppe van der Voort, L., & Löfdahl, M. G. 2005, Sol. Phys., 228, 191
Vecchio, A., Cauzzi, G., & Reardon, K. P. 2009, A&A, 494, 269
Viticchié, B., Del Moro, D., Berrilli, F., Bellot Rubio, L., & Tritschler, A. 2009, ApJ, 700, L145